HAL
open science

Solution of the Population Balance Equation for Two-Component Aggregation by an Extended Fixed Pivot Technique

Hugo Vale, Timothy Mckenna

To cite this version:

Hugo Vale, Timothy Mckenna. Solution of the Population Balance Equation for Two-Component Aggregation by an Extended Fixed Pivot Technique. Industrial and engineering chemistry research, 2005, 44, pp.7885-7891. 10.1021/ie050179s . hal-00004523v2

HAL Id: hal-00004523

https://hal.science/hal-00004523v2

Submitted on 24 Nov 2005

HAL is a multi-disciplinary open access archive for the deposit and dissemination of scientific research documents, whether they are published or not. The documents may come from teaching and research institutions in France or abroad, or from public or private research centers.

L'archive ouverte pluridisciplinaire **HAL**, est destinée au dépôt et à la diffusion de documents scientifiques de niveau recherche, publiés ou non, émanant des établissements d'enseignement et de recherche français ou étrangers, des laboratoires publics ou privés.

Solution of the Population Balance Equation for Two-Component Aggregation by an Extended Fixed Pivot Technique

Hugo M. Vale and Timothy F. McKenna*

CNRS-LCPP/ESCPE-Lyon, BP 2077, 43 Blvd du 11 novembre 1918, 69616 Villeurbanne Cedex, France

*Tel.: +33-4-724-31775; Fax: +33-4-724-31768; E-mail: mckenna@cpe.fr

Abstract

The fixed pivot technique of Kumar and Ramkrishna (*Chem. Eng. Sci.*, **1996**, *51* (8), 1311-1332), originally derived for one-dimensional systems, is extended to simulate two-component aggregation processes. By following this approach, it is possible to design a numerical method that guarantees internal consistency with regard to certain moments of the distribution, while using arbitrary Cartesian grids. Focus is put on achieving internal consistency with respect to the number of particles and the mass of each component, although other moments may be considered if desired. The potentialities and limitations of the technique are evaluated by comparing the numerical solutions against available analytical solutions. This comparison reveals that the proposed method is rather accurate, except in the front region, which shows some smearing. The accuracy, internal consistency, and computational efficiency of this numerical method should make it a valuable tool for simulating two-component aggregation.

Keywords

Aggregation; Coagulation; Multicomponent; Particle size distribution; Population balance.

1. Introduction

Simulating the dynamics of multicomponent aggregation is of interest in a number of fields, such as chemical engineering[1,2], aerosol and atmospheric science[3], medical research[4], etc. The simplest case one may encounter, but nevertheless important, is obviously that of a two-component system. If the system is spatially homogeneous, the aggregation process is described by the following population balance equation (PBE)[1,5]

$$\begin{aligned}\frac{\partial n(x,y,t)}{\partial t} &= \frac{1}{2}\int_0^x\int_0^y b(x-x',y-y';x',y';t)\,n(x-x',y-y',t)\,n(x',y',t)dx'dy' \\ &\quad - n(x,y,t)\int_0^\infty\int_0^\infty b(x,y;x',y';t)\,n(x',y',t)dx'dy'\end{aligned} \tag{1}$$

where $n(x,y,t)\,dx\,dy$ is the number of particles of state (x,y) per unit volume at time t and $b(x,y;x',y';t)$ is the aggregation rate coefficient. The internal coordinates x and y denote the amount (mass, moles, etc.) of each component in the particle.

The resolution of PBEs such as eq 1 still raises a number of difficulties. The reader is referred to Obrigkeit et al.[1,2] for an up-to-date review of methods for solving multicomponent PBEs. Basically, one may distinguish between methods capable of determining the full size-composition distribution and simpler methods based on approximate representations of the variations in particle composition. The second class of algorithms has a lower computational cost (they often scale linearly with the number of components), but of course, some information on the composition distribution is lost along with the reduction in dimensionality.

There are not many methods available in the literature to determine the full size-composition distribution in multicomponent aggregation processes. Kim and Seinfeld[3] proposed a finite element scheme for simulating aggregation and growth in multicomponent systems. Despite its generality, when employed to describe pure coagulation, this method fails to conserve the mass of each component and discrepancies are observed in the predictions for the number of particles. This is a serious limitation, as the accurate computation of such quantities is essential for obtaining physically coherent solutions. The other alternative is Monte Carlo methods, such as the one developed by Laurenzi et al.[4] These algorithms are very accurate and efficient, but several sets of simulations must be performed in order to obtain values for the number density function.

In contrast, several numerical techniques have been proposed for simulating aggregation in one-dimensional systems. Among the various discretization schemes developed (see Vanni[6] for a review), the fixed pivot technique of Kumar and Ramkrishna[7] has emerged as one of the best, being robust, versatile, accurate, and simple to implement. According to this method, the size domain is subdivided into contiguous cells, with the particles in each cell being concentrated at a representative size (the pivot). If the size of a particle formed by aggregation does not fall on any pivot, the new particle is assigned to the two nearby pivots. The fractional particle attributed to each pivot is determined in such a way that two properties of interest are exactly preserved. It is the ability to work with arbitrary grids and the capacity to ensure internal consistency with regard to any two moments of the distribution (typically number and mass) that made this method so well-accepted and widely used.

Our goal in this work is to develop a new technique for determining the full size-composition distribution in two-component aggregation processes that possesses the

advantages of the approach by Kumar and Ramkrishna[7]. In the following section, the proposed technique is described in detail. In Section 3, the performance of the method is demonstrated by comparing the numerical results with analytical solutions for pure aggregation in multicomponent systems. Conclusions are drawn in Section 4.

2. Formulation of the Discrete Equations

We will assume a Cartesian grid, i.e., the computational domain is a rectangle $[x_{\min}, x_{\max}]\times[y_{\min}, y_{\max}]$ covered by cells $C_{ij} \equiv [x_{i-1/2}, x_{i+1/2}]\times[y_{i-1/2}, y_{i+1/2}]$ with $1 \le i \le M_x$ and $1 \le j \le M_y$. The representative coordinates (the pivots) of the population in cell C_{ij} are denoted (x_i, y_j). For the sake of clarity, a typical grid is shown in Figure 1. It is worth stressing that the grid may be nonregular in both coordinates.

As explained in Section 1, in the fixed pivot technique for one-dimensional distributions, a new particle is assigned to the two nearby pivots and the two unknown fractions are determined by imposing the conservation of an equal number of properties. Clearly, to generalize this approach to bidimensional distributions, the first issue that must be addressed is which pivots will be used and, consequently, what properties will be conserved.

In this work, we empirically adopted what is perhaps the most intuitive option. We selected the four pivots surrounding a new particle, i.e., the points $\{(x_i, y_j), (x_i, y_{j+1}), (x_{i+1}, y_j), (x_{i+1}, y_{j+1})\}$ such that $x_i < \hat{x} < x_{i+1}$ and $y_j < \hat{y} < y_{j+1}$, where $(\hat{x}, \hat{y})$ are the internal coordinates of the new particle. This is depicted in Figure 2. Thus, we have four fractions *a*, *b*, *c* and *d* that are to be determined from the preservation of four properties. We note that the pivots may be chosen in other ways. However, this selection has been shown to be both efficient and easy to implement.

Following Kumar and Ramkrishna[7], the fractions *a*, *b*, *c* and *d* assigned to each pivot (see Figure 2) are computed by imposing the conservation of four properties $f_n(x, y)$,

$$f_n(\hat{x},\hat{y}) = a\, f_n(x_i, y_j) + b\, f_n(x_{i+1}, y_j) + c\, f_n(x_i, y_{j+1}) + d\, f_n(x_{i+1}, y_{j+1}) \qquad (2)$$

where $n = \{1,2,3,4\}$. Note, however, that these properties cannot be chosen arbitrarily, since our set of pivotal points only contains two distinct values of *x* and *y*. In other words, the properties must be chosen in such a way that the coefficient matrix of the above linear system of equations is nonsingular. For instance, we cannot simultaneously conserve the power-law properties: x, x^2, y and y^2. Fortunately, for a large majority of applications, this constraint is not a limiting factor. In fact, as mentioned in the introductory section, the main concern is usually to achieve internal consistency with regard to the number of particles and the mass of each component, which is perfectly compatible with the method here described. For such cases, the most interesting set of properties is likely to be the following:

$$\begin{cases} f_1(x,y) = 1 \\ f_2(x,y) = x \\ f_3(x,y) = y \\ f_4(x,y) = xy \end{cases} \qquad (3)$$

If the state vector is $(x,y) = (m_1, m_2)$, the first three expressions correspond to the conservation of the number of particles and the mass of each component, respectively. The choice of a fourth property is not evident. Here, we have adopted the first cross moment. First, because it is logical to employ an expression that gives equal importance to both components. Second, because the preservation of the first cross moment ensures that we get a balanced distribution of the particles among the four pivots. In fact, adding the fourth property is equivalent to imposing the condition $ad = bc$.

According to the assignment scheme described above, it is easy to see that the pivot (x_i, y_j) will receive a contribution for every particle born in any of the four surrounding rectangles (see Figure 2). That is, for every particle born in the region $R_{ij} \equiv \{(x,y): x_{i-1} < x < x_{i+1}, y_{j-1} < y < y_{j+1}\}$. The actual fraction can be determined by solving eq 2 for the relevant points. If we consider the properties given in eq 3, this fraction reads:

$$h_{ij}(\hat{x},\hat{y}) = \begin{cases} \dfrac{(\hat{x}-x_{i-1})(\hat{y}-y_{j-1})}{(x_i-x_{i-1})(y_j-y_{j-1})}, & x_{i-1} \le \hat{x} \le x_i \wedge y_{j-1} \le \hat{y} \le y_j \\ \dfrac{(x_{i+1}-\hat{x})(\hat{y}-y_{j-1})}{(x_{i+1}-x_i)(y_j-y_{j-1})}, & x_i \le \hat{x} \le x_{i+1} \wedge y_{j-1} \le \hat{y} \le y_j \\ \dfrac{(\hat{x}-x_{i-1})(y_{j+1}-\hat{y})}{(x_i-x_{i-1})(y_{j+1}-y_j)}, & x_{i-1} \le \hat{x} \le x_i \wedge y_j \le \hat{y} \le y_{j+1} \\ \dfrac{(x_{i+1}-\hat{x})(y_{j+1}-\hat{y})}{(x_{i+1}-x_i)(y_{j+1}-y_j)}, & x_i \le \hat{x} \le x_{i+1} \wedge y_j \le \hat{y} \le y_{j+1} \end{cases} \tag{4}$$

We are now ready to formulate the discrete equations for a two-component aggregation process. Following Kumar and Ramkrishna[7], we define $N_{ij}(t)$ as the number of particles in cell C_{ij} at time *t*,

$$N_{ij}(t) = \iint_{C_{ij}} n(x,y,t)\,dx\,dy \tag{5}$$

and then express the number density function as,

$$n(x,y,t)=\sum_{i,j}N_{ij}(t)d(x-x_i,y-y_j) \tag{6}$$

since the particles in cell C_{ij} are assumed to be concentrated at the pivotal point (x_i,y_j). Recalling that the cell C_{ij} receives a fraction h_{ij} for every particle formed in the region R_{ij}, we can integrate eq 1 to obtain:

$$\begin{aligned}\frac{dN_{ij}(t)}{dt}=&\frac{1}{2}\iint_{R_{ij}}dx\,dy\,h_{ij}(x,y)\int_0^x\int_0^y b(x-x',y-y';x',y';t)\,n(x-x',y-y',t)\,n(x',y',t)dx'dy'\\&-\iint_{C_{ij}}dx\,dy\,n(x,y,t)\int_0^\infty\int_0^\infty b(x,y;x',y';t)\,n(x',y',t)dx'dy'\end{aligned} \tag{7}$$

Replacing $n(x,y,t)$ according to eq 6, and after some manipulations to process the Dirac deltas, we obtain the following equations (see Appendix A)

$$\begin{aligned}\frac{dN_{ij}}{dt}&=\sum_{\{k,l,q,r\}\in\Omega_{ij}}(1-\tfrac{1}{2}d_{kq}d_{lr})h_{ij}(\hat{x},\hat{y})b_{kl,qr}N_{kl}N_{qr}-N_{ij}\sum_{k,l}b_{ij,kl}N_{kl}\\ \Omega_{ij}&=\{\{k,l,q,r\}:1\le k\le i,1\le l\le j,l\le r\le j,1+d_{rl}(k-1)\le q\le i,(\hat{x},\hat{y})\in R_{ij}\}\end{aligned} \tag{8}$$

where

$$b_{ij,kl}=b(x_i,y_j;x_k,y_l;t) \tag{9}$$

and d_{ij} is the Kronecker delta.

The discretized PBE, eq 8, is a natural extension of the one-dimensional expression given by Kumar and Ramkrishna[7]. The possible (nonrepeated) combinations of cells C_{kl} and C_{qr} leading to the formation of a new particle in the region R_{ij} are computed only once, at the moment of grid generation. Likewise, the values of $h_{ij}(\hat{x}, \hat{y})$, which are time-independent, are calculated at the beginning of the computations and then stored in an interaction matrix, as suggested by Attarakih et al.[8]

3. Numerical Results

In this section, the performance of the proposed numerical technique is evaluated by testing it for cases that can be solved analytically. At present, the only analytical solutions available[4,9,10] for the two-component aggregation PBE refer to a constant aggregation kernel, $b = b_0$. Lushnikov[9] first solved the aggregation equation for a binary system, assuming an exponential initial distribution. Later, Gelbard and Seinfeld[10] generalized Lushnikov's treatment and obtained solutions of the multicomponent PBE including both coagulation and growth for a general class of initial conditions. Recently, Laurenzi et al.[4] presented an analytical solution for an initial distribution with two types of pure, exponentially distributed particles.

Here, we will compare our numerical results with the analytical solutions derived by Gelbard and Seinfeld[10] for two different types of initial distribution. Similar results, in qualitative and quantitative terms, were found for the initial conditions used by Lushnikov[9] and Laurenzi et al.[4] In terms of the mass of each component, the distributions considered are the following

$$n(m_1, m_2, 0) = \frac{16N_0}{m_{10}m_{20}}\left(\frac{m_1}{m_{10}}\right)\left(\frac{m_2}{m_{20}}\right)\exp\left(-2\frac{m_1}{m_{10}} - 2\frac{m_2}{m_{20}}\right) \tag{10}$$

$$n(m_1, m_2, 0) = \frac{4N_0}{m_{10}m_{20}}\left(\frac{m_1}{m_{10}}\right)\exp\left(-2\frac{m_1}{m_{10}} - \frac{m_2}{m_{20}}\right) \tag{11}$$

where N_0 is the initial number of particles per unit volume, and m_{i0} is the initial mean mass of the *i*th component in a particle. The analytical solutions corresponding to both these initial conditions are given in Appendix B.

The comparison between numerical and analytical results is done in terms of the cell average number density, $\bar{n}_{ij}(t)$, plotted at the pivotal coordinates. The numerical average value can be directly computed from the N_{ij}'s,

$$\bar{n}_{ij}(t) = \frac{N_{ij}(t)}{\Delta x_i \Delta y_j} \tag{12}$$

while the analytical value is determined from the integration of the analytical solution,

$$\bar{n}_{ij}(t) = \frac{1}{\Delta x_i \Delta y_j} \iint_{C_{ij}} n(x, y, t)\, dx\, dy \tag{13}$$

where $\Delta x_i = x_{i+1/2} - x_{i-1/2}$ and $\Delta y_j = y_{j+1/2} - y_{j-1/2}$ denote the grid sizes.

Let us start by analyzing the results for a system with an initial distribution described by eq 10 (case study 1). For this first case study, a 40×40 geometrical grid was used and the following parameters were considered: $N_0 = 1$, $m_{10} = 1$ and $m_{20} = 5$. We note that all of the numerical results reported throughout this work were obtained by imposing the preservation of the properties given in eq 3, i.e., with h determined from eq 4. Also, the ordinary differential equations were integrated with LSODE[11] (Adams method, RTOL=10^{-4} and ATOL=10^{-18}).

A contour plot of the numerical solution at $t = 100$ ($t = N_0 b_0 t$) is depicted in Figure 3. In addition, Figure 4 presents a comparison of the numerical and analytical values of the cell average number density, along the grid diagonal, for three dimensionless times.

The three time instants correspond to aggregation extents of 71, 93 and 98%, respectively. In this log-log plot, the abscissa axis represents the m_1 value of each pivot. As shown in Figure 4, the agreement between numerical and analytical results is globally good. Nevertheless, there is an observable mismatch in the front region, which tends to augment with the extent of aggregation: we can distinguish both zones of under- and overprediction. In fact, what we observe is that the front is somewhat smeared with respect to the actual solution. As a result of this smearing (or numerical diffusion) effect, there is a systematic overprediction of the number density function in the high mass range. At the same time, since the number of particles (the volume under the bivariate surface) is correctly evaluated, there is a consequent under estimation of the number density function around the peaks or crests of the distribution.

In Figure 5, we compare numerical and analytical results for the evolution of the moments of the distribution, up to order three. Note that the moments were normalized with respect to their initial value. The analytical expressions are given in Appendix B. Additionally, the relative error in the moments at $t = 100$, for different grids, is summarized in Table 1. As expected, the moments $M_{0,0}$, $M_{1,0}$, $M_{0,1}$, and $M_{1,1}$ are accurately predicted. With regard to the remaining moments, reasonable agreement is achieved, taking into consideration the evolution over several orders of magnitude. The over estimation of the moments, evidenced in Table 1, is a consequence of the aforementioned smearing of the front.

The results for a system with an initial distribution described by eq 11 (case study 2) are analogous. For this second case study, we considered the following parameters: $N_0 = 1$ and $m_{10} = m_{20} = 1$. Again, a 40×40 geometrical grid was employed. Figure 6 presents the

outcome of a simulation for $t = 100$, while Figure 7 compares the values of the cell average number density along the grid diagonal. As before, the numerical and analytical solutions are in good agreement, but the smearing of the front is again visible. The evolution of the first moments of the distribution is depicted in Figure 8. The number of particles, the mass of each component, and the first cross moment are correctly evaluated. The deviations found in the other moments are identical to those reported for the first case study (see Table 1).

The smearing of the advancing front is most probably due to the fact that this approach neglects the variation of the number density function within the cells, as described by other authors[7,12,13] for one-dimensional distributions. This adverse effect leads to deviations in the number density function and to an over estimation of the high order moments. One way to minimize the inconveniences of numerical diffusion is to increase the number of grid points, as shown in Table 1. Of course, this increases the computation time (see Table 2). Alternatively, one may use a grid denser in the front zone. Inferring from the analysis of Kumar and Ramkrishna[7], the discrepancies in the front are likely to increase with the degree of homogeneity of the kernel. Unfortunately, we cannot quantify these deviations, since no analytical solutions exist for nonconstant kernels.

The ability to preserve number and mass is a key feature of the proposed numerical technique. For instance, in comparison to the finite element scheme of Kim and Seinfeld[3], our technique is found to be clearly superior. The latter method shows nonnegligible losses in both number (7%) and mass of particles (8%), even for $t = 1$. Obviously, with such a method, the predictions of higher moments and for higher extents of aggregation would be even worse and, thus, physically unacceptable.

Finally, for practical applications, it is of the utmost importance that the numerical method is efficient in terms of both accuracy and CPU time. To illustrate the requirements of the algorithm in terms of solution time, two situations were considered, having the same initial distribution but aggregation kernels of distinct complexity. The first situation corresponds to case study 1, which represents an idealized kernel. The second situation (case study 3) corresponds to a more realistic kernel, dependent on particle size and composition. For the latter, we chose the following Brownian-like kernel[4]

$$b(m_1, m_2; m_1', m_2'; t) = e\, b_0 \left(2 + \left(\frac{m}{m'} \right)^{1/3} + \left(\frac{m'}{m} \right)^{1/3} \right) \tag{14}$$

with

$$e = f_1 f_1' e_{11} + (f_2 f_1' + f_1 f_2') e_{12} + f_2 f_2' e_{22} \tag{15}$$

where m is the total mass of a particle, e is the sticking probability between two particles, e_{ij} is the sticking probability between pure particles of components i and j, and f_i is the mass fraction of component i in a particle. Note that, for simplicity, we assumed particle density to be independent of composition in the above equations. The e_{ij}'s were taken as: $e_{11} = 0.8$, $e_{12} = 0.6$, and $e_{22} = 0.1$.[4] Figure 9 depicts the contour plot for this case study.

The CPU times obtained on a 2.4-GHz PC for case studies 1 and 3 are summarized in Table 2. We can see that although case study 3 is more time-consuming (ca. 2 times), the solution times are on the same order of magnitude in both cases. We also observe that the computing time increases substantially with the number of grid points, approximately as

$(M_x M_y)^{2.5}$ in both cases. Nevertheless, CPU times of this magnitude are perfectly affordable even with a desktop PC, therefore, demonstrating that the proposed numerical technique is a viable option for simulating two-component aggregation processes.

4. Conclusions

In this article, we extended the fixed pivot technique of Kumar and Ramkrishna[7] to the solution of the PBE for two-component aggregation. A new particle that does not match with any of the existing pivots is assigned to the four surrounding pivots. The fractions allocated to each pivot are determined by imposing the preservation of four properties. The technique is applicable to Cartesian grids, eventually nonregular in both coordinates.

Detailed expressions were given for ensuring the conservation of the number of particles, the mass of each component, and the first cross moment, although other moments may be considered if desired (within the restrictions mentioned). The performance of the algorithm was evaluated by comparing the numerical results with analytical solutions for a constant aggregation kernel (the only available). Numerical and analytical solutions were found to agree rather well, except in the front zone, where the original technique also presents some deviations. Moreover, higher-order moments of the distribution were reasonably well-predicted.

The proposed numerical technique fulfills the characteristics required for the simulation of actual two-component aggregation processes. Accurate, efficient, and capable of determining the full size-composition distribution for binary systems, the method is a good alternative or complement to other techniques. With respect to methods based on approximate descriptions of the composition, more information is obtained in exchange of higher, but affordable, CPU times. One could also think of further extending the fixed pivot approach to higher dimensions. Although this is perfectly possible from a theoretical point of view, in practice, the computational cost of solutions of this type would be quite significant. For more than two components, approximate methods or Monte Carlo algorithms would most probably be preferred.

Acknowledgment

Hugo M. Vale wishes to thank the Portuguese Science and Technology Foundation for financial support (grant SFRH/BD/10513/2002).

Appendix A. Derivation of Equation 8

Starting with the birth term of eq 7 and making use of eq 6, we obtain

$$\left.\frac{dN_{ij}}{dt}\right|_{\text{birth}} = \frac{1}{2}\iint_{R_{ij}} dx\,dy\,h_{ij}(x,y)\int_0^x\int_0^y dx'dy'\,b(x-x',y-y';x',y')\times \\ \times\sum_{k,l,q,r} N_{kl}N_{qr}\,d(x-x'-x_k,y-y'-y_l)\,d(x'-x_q,y'-y_r) \tag{A1}$$

where, for simplicity, the two sum operators have been condensed into a single one. We now interchange the order of integration and summation to get

$$\left.\frac{dN_{ij}}{dt}\right|_{\text{birth}} = \frac{1}{2}\sum_{k,l,q,r}\iint_{R_{ij}} dx\,dy\,h_{ij}(x,y)\int_0^x\int_0^y dx'dy'\,b(x-x',y-y';x',y')\times \\ \times N_{kl}N_{qr}\,d(x-x'-x_k,y-y'-y_l)\,d(x'-x_q,y'-y_r) \tag{A2}$$

Applying the shifting property of the Dirac delta function, we find that the only nonzero terms of the sum are those for which $(\hat{x},\hat{y}) \equiv (x_k + x_q, y_l + y_r) \in R_{ij}$ and, thus,

$$\left.\frac{dN_{ij}}{dt}\right|_{\text{birth}} = \frac{1}{2}\sum_{\{k,l,q,r\}\in\Omega_{ij}} h_{ij}(\hat{x},\hat{y})\,b(x_k,y_l;x_q,y_r)\,N_{kl}N_{qr} \\ \Omega_{ij} = \{\{k,l,q,r\}: 1\le k,q\le i; 1\le l,r\le j; (\hat{x},\hat{y})\in R_{ij}\} \tag{A3}$$

Finally, this symmetrical sum can be further simplified by removing the repeated combinations, resulting in

$$\left.\frac{dN_{ij}}{dt}\right|_{\text{birth}} = \sum_{\{k,l,q,r\}\in\Omega_{ij}} (1-\tfrac{1}{2}d_{kq}d_{lr})h_{ij}(\hat{x},\hat{y})b(x_k,y_l;x_q,y_r)N_{kl}N_{qr}$$

$$\Omega_{ij} = \{\{k,l,q,r\}: 1\le k\le i, 1\le l\le j, l\le r\le j, 1+d_{rl}(k-1)\le q\le i, (\hat{x},\hat{y})\in R_{ij}\} \tag{A4}$$

A similar reasoning is used for the death term. Again, we make use of eq 6 to obtain

$$\left.\frac{dN_{ij}}{dt}\right|_{\text{death}} = -\iint_{C_{ij}} dx\,dy\, N_{ij} d(x-x_i, y-y_j)\times \\ \times\int_0^\infty\int_0^\infty b(x,y;x',y')\sum_{k,l} N_{kl} d(x'-x_k, y'-y_l)\,dx'dy' \tag{A5}$$

and then interchange the order of integration and summation to get

$$\left.\frac{dN_{ij}}{dt}\right|_{\text{death}} = -\iint_{C_{ij}} dx\,dy\, N_{ij} d(x-x_i, y-y_j)\times \\ \times\sum_{k,l}\int_0^\infty\int_0^\infty b(x,y;x',y')N_{kl} d(x'-x_k, y'-y_l)dx'dy' \tag{A6}$$

Finally, by using the shifting property of the Dirac delta function, we arrive at

$$\left.\frac{dN_{ij}}{dt}\right|_{\text{death}} = -N_{ij}\sum_{k,l} b(x_i,y_j;x_k,y_l)N_{kl} \tag{A7}$$

Appendix B. Analytical Solutions

B.1. Initial Condition: Eq 10. For a constant aggregation coefficient $b = b_0$, the exact solution of eq 1, subject to the initial condition eq 10, reads[10]

$$n(m_1, m_2, t) = \frac{8N_0}{m_{10} m_{20} \sqrt{t\,(t+2)^3}} \exp\left(-2\frac{m_1}{m_{10}} - 2\frac{m_2}{m_{20}} \right) \left(I_0(q) - J_0(q) \right) \qquad \text{(B1)}$$

with:

$$q = 4\left(\frac{m_1 m_2}{m_{10} m_{20}} \right)^{1/2} \left(\frac{t}{t+2} \right)^{1/4} \qquad \text{(B2)}$$

Here, $t = N_0 b_0 t$ is the dimensionless time, and $J_n(q)$ and $I_n(q)$ are, respectively, the Bessel function and the modified Bessel function of the first kind. The moments of the distribution $M_{i,j}$ are defined by

$$M_{i,j}(t) = \int_0^\infty \int_0^\infty x^i y^j n(x, y, t)\, dx dy \qquad \text{(B3)}$$

For this solution, the first moments, up to order three, are

$$M_{0,0}(t) = 2N_0 / (2 + t) \qquad \text{(B4)}$$

$$M_{1,0}(t) = m_{10} N_0 \qquad \text{(B5)}$$

$$M_{2,0}(t) = \tfrac{1}{2} m_{10}^2 N_0 (3 + 2t) \tag{B6}$$

$$M_{1,1}(t) = m_{10} m_{20} N_0 (1 + t) \tag{B7}$$

$$M_{3,0}(t) = \tfrac{3}{2} m_{10}^3 N_0 (1 + t)(2 + t) \tag{B8}$$

$$M_{2,1}(t) = \tfrac{1}{2} m_{10}^2 m_{20} N_0 (3 + 7t + 3t^2) \tag{B9}$$

The moment $M_{j,i}$ can be obtained from $M_{i,j}$ by transposing m_{10} and m_{20}.

B.2. Initial Condition: Eq 11. For a constant aggregation coefficient $b = b_0$, the exact solution of eq 1, subject to the initial condition eq 11, is given by the following expression[10]

$$n(m_1, m_2, t) = \frac{16 N_0}{m_{10} m_{20} (t + 2)^2} \exp\left(-2 \frac{m_1}{m_{10}} - \frac{m_2}{m_{20}} \right) \sum_{k=0}^{\infty} \frac{\left(\dfrac{4t\, m_2}{(t + 2) m_{20}} \right)^k \left(\dfrac{m_1}{m_{10}} \right)^{2k+1}}{k!(2k+1)!} \tag{B10}$$

which can be evaluated in terms of the generalized hypergeometric function[14]. The moments $M_{0,0}$, $M_{1,0}$, $M_{0,1}$, $M_{2,0}$, $M_{1,1}$, and $M_{3,0}$ are given by the same formulas presented above. The remaining moments are more complex to determine and, thus, were found by the numerical integration of eq B3.

Nomenclature

a, b, c, d = particle fractions

C_{ij} = cell

$f_n(x, y)$ = nth property to be preserved

m = total mass of a particle

m_i = mass of component i in a particle

m_{i0} = initial mean mass of component i in a particle

M = number of cells along a given coordinate

$M_{i,j}$ = mixed moment of the number density function

$n(x, y, t)\,dx\,dy$ = number of particles of state (x, y) per unit volume at time t

$\overline{n}_{ij}$ = average number density in cell C_{ij}

N_0 = initial number of particles per unit volume

N_{ij} = number of particles in cell C_{ij}

t = time

x, y = internal coordinates

x_i, y_j = pivotal coordinates

$\hat{x}, \hat{y}$ = coordinates of a new particle

Greek Letters

b = aggregation rate coefficient

e = sticking probability between particles

e_{ij} = sticking probability between pure particles of component *i* and *j*

f_i = mass fraction of component *i* in a particle

h_{ij} = particle fraction assigned to pivot (x_i, y_j)

t = dimensionless time

Literature Cited

(1) Obrigkeit, D. D.; McRae, G. J., Integrated framework for the numerical solution of multicomponent population balances. 1. Formulation, representation, and growth mechanisms. *Ind. Eng. Chem. Res.* **2004**, *43*, 4380-4393.

(2) Obrigkeit, D. D.; Resch, T. J.; McRae, G. J., Integrated framework for the numerical solution of multicomponent population balances. 2. The split composition distribution method. *Ind. Eng. Chem. Res.* **2004**, *43*, 4394-4404.

(3) Kim, Y. P.; Seinfeld, J. H., Simulation of multicomponent aerosol dynamics. *J. Colloid Interface Sci.* **1992**, *149* (2), 425-449.

(4) Laurenzi, I. J.; Bartels, J. D.; Diamond, S. L., A general algorithm for exact simulation of multicomponent aggregation processes. *J. Comput. Phys.* **2002**, *177*, 418-449.

(5) Ramkrishna, D., *Population balances. Theory and applications to particulate systems in engineering*. Academic Press: San Diego, 2000.

(6) Vanni, M., Approximate population balance equations for aggregation-breakage processes. *J. Colloid Interface Sci.* **2000**, *221*, 143-160.

(7) Kumar, S.; Ramkrishna, D., On the solution of population balance equations by discretization - I. A fixed pivot technique. *Chem. Eng. Sci.* **1996**, *51* (8), 1311-1332.

(8) Attarakih, M. M.; Bart, H.-J.; Faqir, N. M., Numerical solution of the spatially distributed population balance equation describing the hydrodynamics of interacting liquid-liquid dispersions. *Chem. Eng. Sci.* **2004**, *59*, 2567-2592.

(9) Lushnikov, A. A., Evolution of Coagulating Systems III. Coagulating mixtures. *J. Colloid Interface Sci.* **1976**, *54* (1), 94-101.

(10) Gelbard, F.; Seinfeld, J. H., Coagulation and growth of a multicomponent aerosol. *J. Colloid Interface Sci.* **1978**, *63* (3), 472-479.

(11) Hindmarsh, A. C., ODEPACK: a systematized collection of ODE solvers. In *Scientific Computing*, Stepleman, R. S., Ed. North Holland: Amsterdam, 1983; pp 55-64.

(12) Kumar, S.; Ramkrishna, D., On the solution of population balance equations by discretization - II. A moving pivot technique. *Chem. Eng. Sci.* **1996**, *51* (8), 1333-1342.

(13) Trautmann, T.; Wanner, C., A fast and efficient modified sectional method for simulating multicomponent collisional kinetics. *Atmos. Environ.* **1999**, *33*, 1631-1640.

(14) Abramowitz, M.; Stegun, I. A., *Handbook of mathematical functions*. Dover: New York, 1972.

Figure Captions

Figure 1. Typical Cartesian grid, which can be used with the proposed numerical method. The lines denote the cell limits, and the dots denote the pivots.

Figure 2. Assignment of a new particle formed by aggregation. The pivot (x_i, y_j) receives a fractional particle for every particle born in the rectangles I, II, III, or IV.

Figure 3. Case study 1. Contour plot of the logarithm of the average number density at $t = 100$. Initial distribution: eq 10. $N_0 = 1$; $m_{10} = 1$; $m_{20} = 5$; $M_x = M_y = 40$; $b = b_0$.

Figure 4. Case study 1. Comparison of the numerical (symbols) and analytical (lines) solutions along the grid diagonal.

Figure 5. Case study 1. Comparison between the numerical (symbols) and analytical (lines) results for the evolution of the moments of the distribution. The moments are normalized with respect to the value at $t = 0$.

Figure 6. Case study 2. Contour plot of the logarithm of the average number density at $t = 100$. Initial distribution: eq 11. $N_0 = 1$; $m_{10} = m_{20} = 1$; $M_x = M_y = 40$; $b = b_0$.

Figure 7. Case study 2. Comparison of the numerical (symbols) and analytical (lines) solutions along the grid diagonal.

Figure 8. Case study 2. Comparison between the numerical (symbols) and analytical (lines) results for the evolution of the moments of the distribution. The moments are normalized with respect to the value at $t = 0$.

Figure 9. Case study 3. Contour plot of the logarithm of the average number density at $t = 100$. Initial distribution: eq 10. $N_0 = 1$; $m_{10} = 1$; $m_{20} = 5$; $M_x = M_y = 40$; b given by eq 14.

Tables

Table 1. Relative error in the moments for case study 1 at $t = 100$ and different grids

	30×30	40×40	50×50
$M_{0,0}$	0.0	0.0	0.0
$M_{1,0}$ & $M_{0,1}$	0.0	0.0	0.0
$M_{2,0}$ & $M_{0,2}$	13.1	7.2	4.3
$M_{1,1}$	0.0	0.0	0.0
$M_{3,0}$ & $M_{0,3}$	45.6	23.5	13.7
$M_{1,2}$ & $M_{2,1}$	13.3	7.3	4.4

Table 2. CPU times (min) at $t = 100$

Grid	Case study 1	Case study 3
30×30	0.3	0.7
40×40	1.3	2.8
50×50	4.0	8.2

Figures

Figure 1:

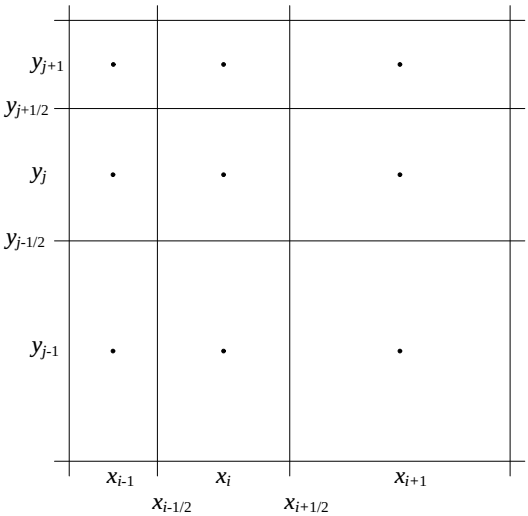

Figure 2:

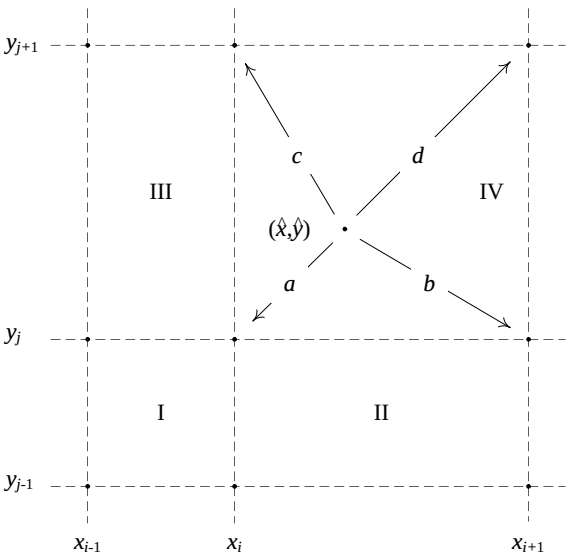

Figure 3:

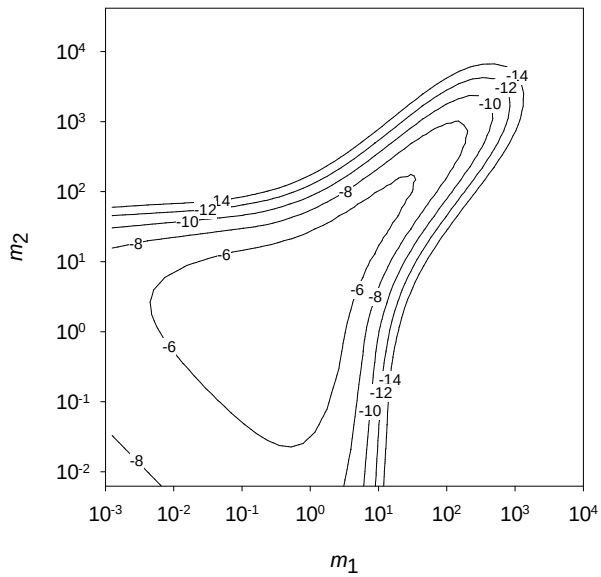

Figure 4:

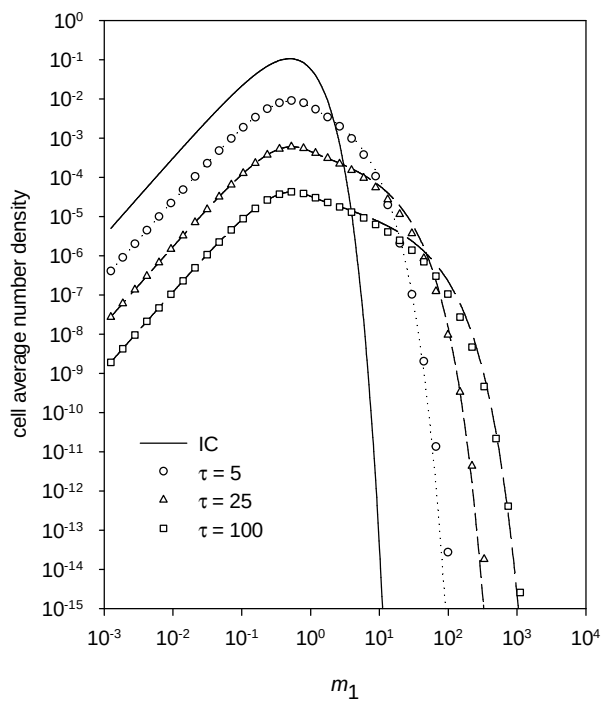

Figure 5:

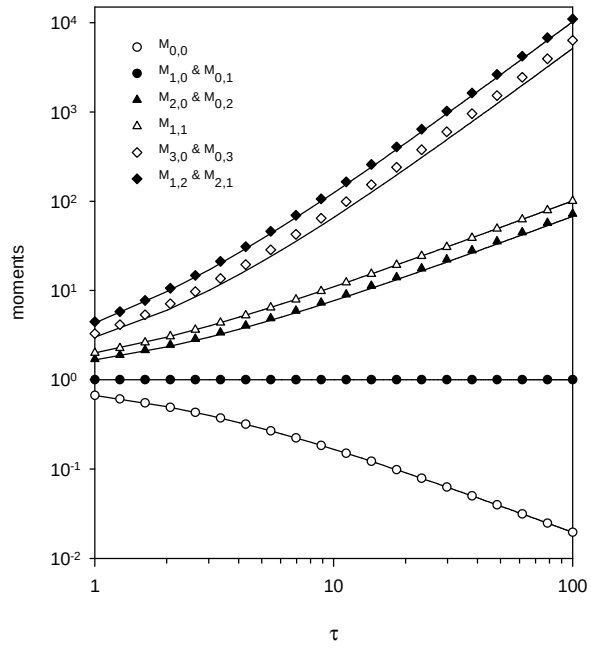

Figure 6:

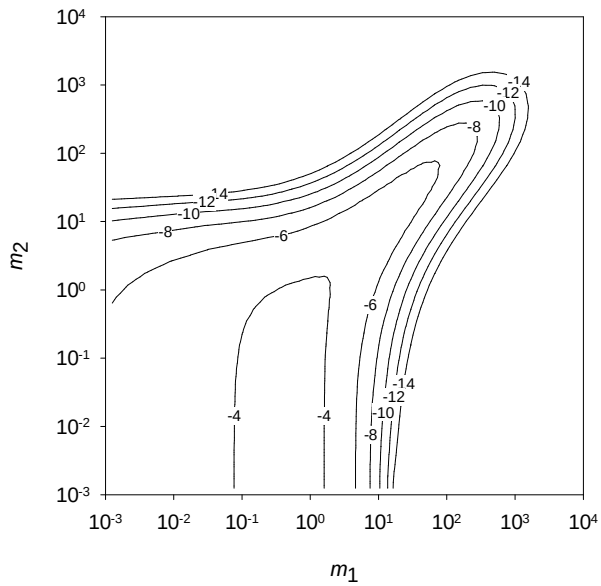

Figure 7:

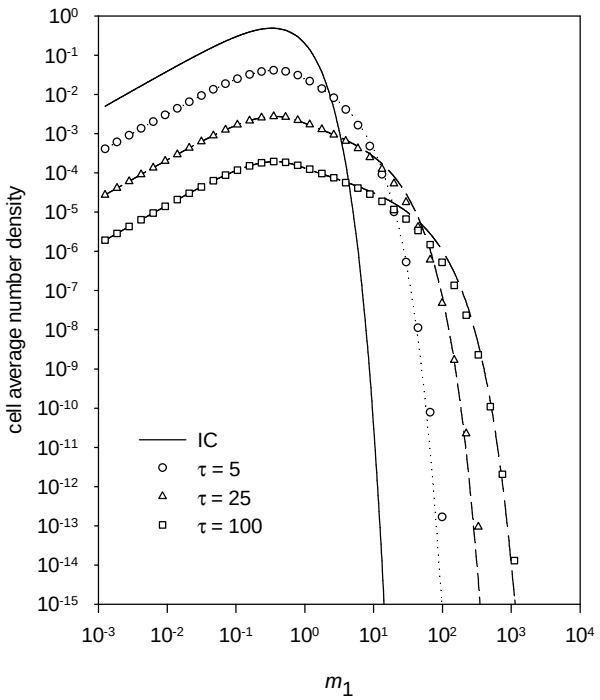

Figure 8:

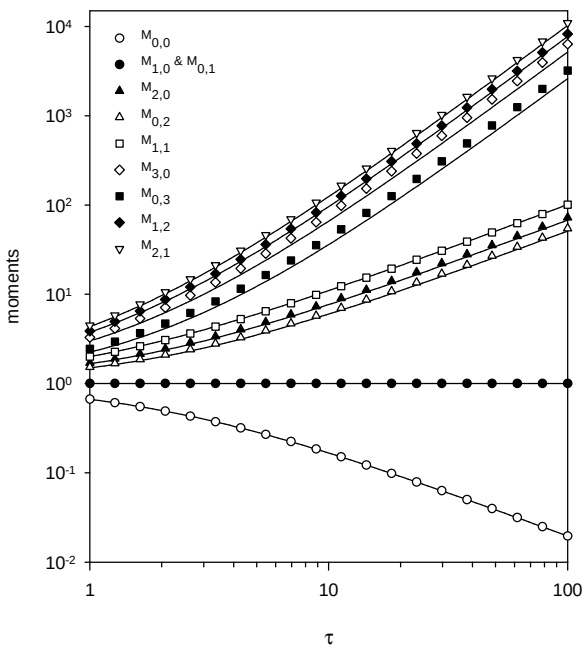

Figure 9:

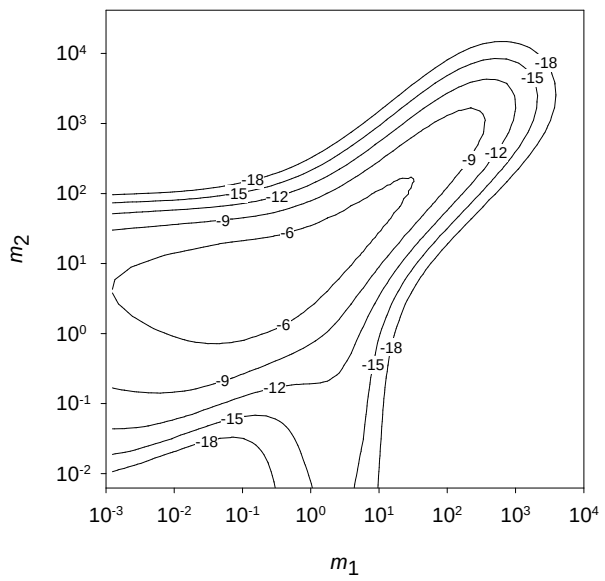
10^4
10^3
10^2
10^1
10^0
10^{-1}
10^{-2}
m_2
10^{-3}
10^{-2}
10^{-1}
10^0
10^1
10^2
10^3
10^4
m_1
-18
-15
-12
-9
-6